Int J Mech Mater Des (2011) 7:149Ð166
DOI 10.1007/s10999-011-9156-4

Micromechanical analysis of fuzzy Þber reinforced composites

S. I. Kundalwal € M. C. Ray

Received: 15 November 2010 / Accepted: 21 April 2011 / Published online: 13 May 2011

Abstract A novel fuzzy Þber reinforced composite (FFRC) reinforced with zig-zag single-walled carbon nanotubes (CNTs) and carbon Þbers is proposed. The distinct constructional feature of this composite is that the uniformly aligned CNTs are radially grown on the surface of carbon Þbers. Analytical models based on the mechanics of materials approach and the Mori–Tanaka method are derived to estimate the effective elastic constants of this proposed FFRC. The values of the effective elastic properties of this composite are estimated with and without considering an interphase between the CNT and the polymer matrix. It has been found that the transverse effective properties of this composite are signiÞcantly improved due to the radial growing of CNTs on the surface of carbon Þber. The effective properties are also found to be sensitive to the CNT diameter.

Keywords Fuzzy Þber composites · Micromechanics · Effective properties · Advanced composites

1 Introduction

Since the discovery of carbon nanotubes (CNTs) (Iijima 1991), researchers have been carrying out extensive work to predict their effective properties. Treacy et al. (1996) experimentally determined that CNTs have axial Young's modulus in the terapascal (TPa) range. Lu (1997) estimated elastic properties of CNTs and nanoropes using an empirical force constant relation. Li and Chou (2003) linked structural and molecular mechanics (SM) approaches to compute elastic properties of CNTs. Shen and Li (2004) reported that CNTs can be modeled as transversely isotropic materials with the axis of transverse isotropy coincident with the centroidal axis of the CNT and developed variational models to determine the values of the Þve elastic constants of CNTs. Xiao et al. (2005) developed an analytical model based on the molecular structural mechanics approach for estimating the mechanical properties of carbon nanotubes. Batra and Sears (2007) proposed that the axis of transverse isotropy of a CNT is a radial line rather than the centroidal axis of the CNT and found that Young's modulus in the radial direction equals about of that in the axial direction. Gupta and Batra (2008) determined the wall thickness and material moduli of a CNT based on the frequencies of axial, torsional, and radial breathing modes. An atomistic-based continuum model has been developed by Cheng et al. (2009) for the estimation of the mechanical properties of single-walled carbon nanotubes.

In order to harness the exceptionally attractive mechanical properties of CNTs, extensive research is being carried out for developing CNT-reinforced composites. For example, Thostenson and Chou

S. I. Kundalwal · M. C. Ray (&)
Department of Mechanical Engineering, Indian Institute of Technology, Kharagpur 721302, India
e-mail: mcray@mech.iitkgp.ernet.in

(2003) have estimated the elastic moduli of CNT-reinforced composite through micromechanical analysis. Using the approach of continuum mechanics, Odegard et al. (2003) predicted the effective elastic moduli of CNT-reinforced composite using an equivalent continuum modeling method. Gou et al. (2004) investigated the interfacial bonding of single-walled carbon nanotubes (SWCNT) reinforced epoxy composites using a combination of computational and experimental methods. Gao and Li (2005) derived a shear lag model of discontinuous CNT-reinforced polymer composites by considering the CNT as an equivalent solid fiber. Song and Youn (2006) numerically estimated the effective elastic properties of CNT-reinforced polymer based composites. Zhang and He (2008) theoretically investigated the viscoelastic behavior of CNT-reinforced composites, developing a three-phase shear lag model. Jiang et al. (2009) determined the maximum volume fraction of CNTs in a CNT-reinforced composite and investigated its effect on the effective elastic properties of the composite. Esteva and Spanos (2009) studied the effect of weakened interfaces between CNTs and the polymer matrix on the effective properties of CNT-reinforced polymer matrix composite. Meguid et al. (2010) developed a model of an atomistic-based representative volume element (RVE) which consists of the CNT, the surrounding epoxy matrix, and the interface between CNT and epoxy to find out effective properties of CNT-reinforced epoxies. They homogenized the RVE into a representative fiber by equating the associated strain energies under identical loading conditions. The same homogenized RVE was then employed in a micromechanical analysis to predict the effective properties of the CNT-reinforced epoxy. Tsai et al. (2010) characterized the elastic properties of CNT-reinforced polymer nanocomposites considering an effective interphase between a CNT and the polymer matrix. Rio et al. (2010) experimentally as well as theoretically investigated the effective properties of CNT-reinforced polyester composites. Wernik and Meguid (2011) presented a nonlinear atomistic-based continuum model for predicting the effective mechanical properties of CNT-reinforced polymer composite. To exploit the attractive elastic properties of CNTs, Ray and Batra (2009) proposed a hybrid piezoelectric composite (HPZC) reinforced with CNTs and piezoelectric fibers. In this HPZC, the CNTs are vertically aligned and parallel to the vertical piezoelectric fibers.

Although a great prospect has been highlighted through the above mentioned in situ research on CNT-reinforced composites, the manufacturing of such unidirectional continuous CNT-reinforced composites in large scale has to encounter some challenging difficulties. Typical among these are the agglomeration of CNTs, the misalignment and the difficulty in manufacturing very long CNTs. Further research on the practical use of CNTs and improving the effective properties of existing fiber-reinforced polymer matrix composites has led to the growth of CNTs on the surface of the advanced fibers. For example, Zhang et al. (2008) produced CNT arrays on the host aluminum silicate and quartz fibers. Mathur et al. (2008) experimentally investigated that the flexural strength and the modulus of the carbon-fiber-reinforced composite can be improved by growing CNTs on the surface of the carbon fibers. Garcia et al. (2008) fabricated a hybrid laminate in which the reinforcements are a woven cloth of alumina fibers with in situ grown CNTs on the surface of the fibers. They demonstrated that both mechanical and electrical properties of such a laminate are enhanced because of the CNTs grown on the surface of the alumina fibers. Ray et al. (2009) carried out a load transfer analysis of short carbon-fiber-reinforced composite in which the aligned CNTs are radially grown on the surface of the carbon fibers. Most recently, Ray (2010) proposed a novel hybrid smart composite which exhibits improved electro-mechanical properties because of the CNTs radially grown on the piezoelectric fibers.

The long fibers of unidirectional continuous fiber reinforced composites may be augmented with CNTs which are radially grown on their surfaces and the resulting long fiber may influence the effective properties of the augmented composites. Such a fiber coupled with radially grown CNTs on its surface is also being named as "fuzzy fiber" (Mathur et al. 2008; Garcia et al. 2008). However, the polymer matrix composite being composed of such long fuzzy fiber reinforcement has not yet been studied. In this paper, a novel continuous unidirectional fuzzy fiber reinforced composite (FFRC) has been proposed. The fuzzy fiber reinforcement of the FFRC is composed of a long carbon fiber where CNTs are radially grown on the surface of the carbon fiber. Analytical models based on the micromechanics paradigm have been derived for predicting the effective elastic properties of this proposed FFRC.

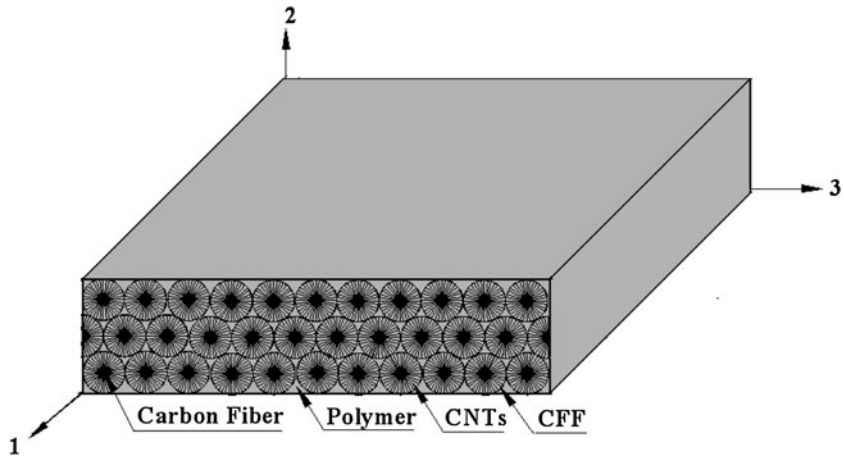

Fig. 1 Schematic diagram of a lamina made of the proposed FFRC

2 Effective elastic properties of the FFRC

Figure 1 shows a schematic sketch of a lamina of the FFRC proposed in this study. The novel constructional feature of such a continuous unidirectional fiber reinforced composite is that CNTs of equal length are uniformly aligned and radially grown on the surface of the carbon fiber reinforcement. CNTs considered here are transversely isotropic (Shen and Li 2004; Tsai et al. 2010). They are grown on the surface of the carbon fibers in such a way that their axes of transverse isotropy are normal to the surface of the carbon fibers. Such a resulting fuzzy fiber (FF) is shown in Fig. 2. When this FF is embedded into the polymer material, the gap between the CNTs is filled with the polymer and the radially aligned CNTs eventually reinforce the polymer matrix surrounding the carbon fiber along the direction transverse to the length of the carbon fiber. Thus the augmented FF can be viewed as a circular cylindrical composite fuzzy fiber (CFF) in which a carbon fiber is embedded in the CNT-reinforced polymer matrix nanocomposite (PMNC) and the diameter of the CFF equals the sum of the diameter of the carbon fiber and the length of a CNT. Such a CFF is schematically demonstrated in Fig. 3. Therefore the RVE of the proposed FFRC can be treated as being composed of two phases wherein the reinforcement is the CFF and the matrix is the polymer material. Thus the analytical procedure for estimating the effective elastic properties of the FFRC starts with the estimation of the effective elastic properties of the PMNC material a priori. Subsequently, considering the PMNC material as the matrix phase and the carbon fiber as the reinforcements, effective elastic properties of the CFF are to be computed. Finally, using the elastic properties of the CFF and the polymer matrix the effective elastic properties of the proposed FFRC can be estimated. Also, CFFs are assumed to be uniformly spaced over the volume of a lamina of the FFRC in such a way that three orthogonal principal material coordinate axes (1-2-3) exist in the proposed composite as shown in Fig. 1. In what follows, micromechanics models for estimating the properties of the PMNC, the CFF and the FFRC will be derived. This section deals with the procedures of employing the two methods, namely, the mechanics of materials (MOM) approach and the Mori-Tanaka (MT) method for estimating the effective elastic properties of the proposed FFRC.

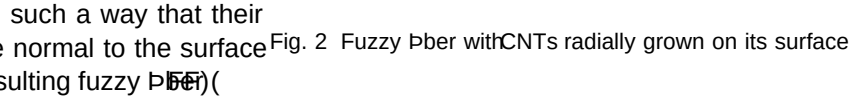

Fig. 2 Fuzzy fiber with CNTs radially grown on its surface

2.1 Mechanics of material (MOM) approach

This section presents the derivation of simple micromechanics models using the MOM approach

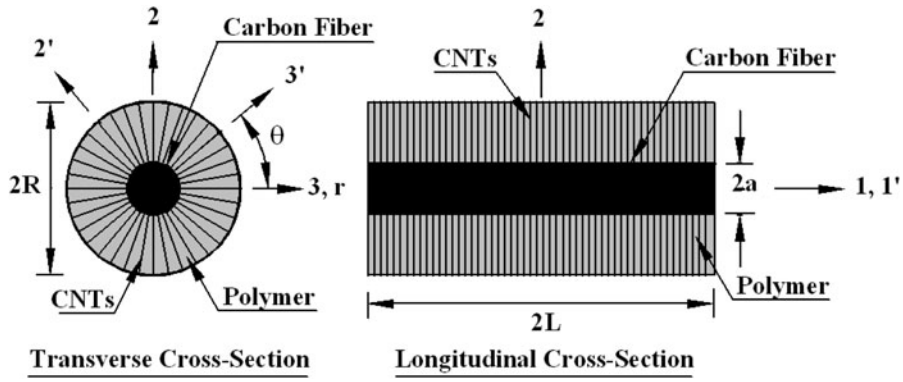

Fig. 3 Transverse and longitudinal cross sections of the CFF

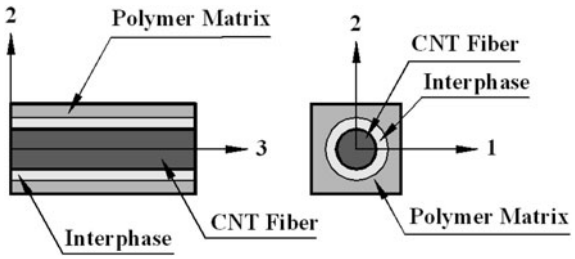

Fig. 4 Cross sections of the RVE of the unwound PMNC material

for estimating the effective elastic properties of the PMNC material surrounding the carbon fiber, the CFF and the FFRC, respectively.

2.1.1 *Effective properties of the PMNC*

As shown in Fig. 3, the constructional feature of the CFF can further be viewed as concentric cylinders in which the carbon fiber is wrapped by a lamina of the PMNC material. Such an unwound lamina of the PMNC is reinforced by CNTs along its thickness direction (i.e., along the 3-direction). The average effective elastic properties of the PMNC material surrounding the carbon fiber may be approximated by estimating the effective elastic properties of this unwound lamina. The cross sections of the RVE (Meguid and Zhu 1995) of this unwound lamina have been shown in Fig. 4. Assuming CNTs as solid fibers (Gao and Li 2005; Tsai et al. 2010), the MOM approach by Ray (2010) can be modified to predict the effective elastic constants C_{ij}^{nc} of the unwound PMNC material. Based on the principal material coordinate (1-2-3) axes shown in Fig. 1, the constitutive relations for the constituent phases of the proposed FFRC are given by

$$\{\sigma^r\} = [C^r]\{\epsilon^r\}; \quad r = f, nt \text{ and } p \tag{1}$$

where the state of stress vector, the state of strain vector and the elastic coefficient matrix of the r^{th} phase are

$$\{\sigma^r\} = \{\sigma_1^r \quad \sigma_2^r \quad \sigma_3^r \quad \sigma_{23}^r \quad \sigma_{13}^r \quad \sigma_{12}^r\}^T,$$

$$\{\epsilon^r\} = \{\epsilon_1^r \quad \epsilon_2^r \quad \epsilon_3^r \quad \epsilon_{23}^r \quad \epsilon_{13}^r \quad \epsilon_{12}^r\}^T,$$

$$[C^r] = \begin{bmatrix} C_{11}^r & C_{12}^r & C_{13}^r & 0 & 0 & 0 \\ C_{12}^r & C_{22}^r & C_{23}^r & 0 & 0 & 0 \\ C_{13}^r & C_{23}^r & C_{33}^r & 0 & 0 & 0 \\ 0 & 0 & 0 & C_{44}^r & 0 & 0 \\ 0 & 0 & 0 & 0 & C_{55}^r & 0 \\ 0 & 0 & 0 & 0 & 0 & C_{66}^r \end{bmatrix} \tag{2}$$

In Eqs. 1 and 2, the superscripts f, nt and p denote, respectively, the carbon fiber, the CNT fiber and the monolithic polymer matrix. For the constituent phase denoted by r, σ_1^r, σ_2^r and σ_3^r are the normal stresses along the principal material coordinate axes 1, 2 and 3, respectively; ϵ_1^r, ϵ_2^r and ϵ_3^r are the corresponding normal strains; σ_{12}^r, σ_{13}^r and σ_{23}^r are the shear stresses; ϵ_{12}^r, ϵ_{13}^r and ϵ_{23}^r are the shear strains and C_{ij}^r $(i, j = 1, 2, 3, \ldots, 6)$ are the elastic coefficients. At this juncture, it is important to mention that several authors (Thostenson and Chou 2003; Gao and Li 2005; Song and Youn 2006; Jiang et al. 2009; Esteva and Spanos 2009) assumed perfectly bonding condition between a CNT and the polymer matrix. Esteva and Spanos (2009) emphatically reported that the

imperfect bonding does not affect the effective longitudinal Young's modulus of the CNT-reinforced polymer matrix composite and marginally affects the transverse properties of the composite for high volume fraction (>0.8) of CNTs. In their extensive research, Tsai et al. (2010) investigated the effect of the interphase between the CNT and the polymer matrix formed due to the non-bonded van der Waals interaction for estimating the effective properties of CNT-reinforced polymer matrix composite. They found that the interphase marginally enhances the effective Young's modulus of the composite transverse to the CNT fiber over that of the composite without the consideration of the interphase. They also estimated the effective properties of the composite considering perfect bonding between the CNT and the surrounding polymer matrix and found them to closely match with the prediction by the molecular dynamics simulation. Hence, in the MOM approach being presented here, it is assumed that CNTs and the polymer matrix are perfectly bonded. In order to satisfy the perfectly bonding situation between the fiber and the matrix, researchers mainly imposed the iso-field conditions and used rules of mixture (Smith and Auld 1991; Bevensite and Dvorak 1992). According to the iso-field conditions one may assume that the normal strains in the homogenized composite, the fiber and the matrix are equal along the fiber direction while transverse stresses in the same phases are equal along the direction transverse to the fiber length. The rules of mixture allow one to express the normal stress along the fiber direction and the transverse strains along the normal to the fiber direction of the homogenized composite in terms of that in the fiber and the matrix and their volume fractions. Such iso-field conditions and rules of mixture (Smith and Auld 1991; Bevensite and Dvorak 1992) for satisfying the perfect bonding conditions between the CNT fiber and the polymer matrix can be expressed as

$$\begin{Bmatrix} \boldsymbol{\sigma}_1^{nt} \\ \boldsymbol{\sigma}_2^{nt} \\ \epsilon_3^{nt} \\ \boldsymbol{\sigma}_{23}^{nt} \\ \boldsymbol{\sigma}_{13}^{nt} \\ \boldsymbol{\sigma}_{12}^{nt} \end{Bmatrix} = \begin{Bmatrix} \boldsymbol{\sigma}_1^{p} \\ \boldsymbol{\sigma}_2^{p} \\ \epsilon_3^{p} \\ \boldsymbol{\sigma}_{23}^{p} \\ \boldsymbol{\sigma}_{13}^{p} \\ \boldsymbol{\sigma}_{12}^{p} \end{Bmatrix} = \begin{Bmatrix} \boldsymbol{\sigma}_1^{nc} \\ \boldsymbol{\sigma}_2^{nc} \\ \epsilon_3^{nc} \\ \boldsymbol{\sigma}_{23}^{nc} \\ \boldsymbol{\sigma}_{13}^{nc} \\ \boldsymbol{\sigma}_{12}^{nc} \end{Bmatrix} \tag{3}$$

and

$$v_{nt} \begin{Bmatrix} \epsilon_1^{nt} \\ \epsilon_2^{nt} \\ \boldsymbol{\sigma}_3^{nt} \\ \epsilon_{23}^{nt} \\ \epsilon_{13}^{nt} \\ \epsilon_{12}^{nt} \end{Bmatrix} + v_p \begin{Bmatrix} \epsilon_1^{p} \\ \epsilon_2^{p} \\ \boldsymbol{\sigma}_3^{p} \\ \epsilon_{23}^{p} \\ \epsilon_{13}^{p} \\ \epsilon_{12}^{p} \end{Bmatrix} = \begin{Bmatrix} \epsilon_1^{nc} \\ \epsilon_2^{nc} \\ \boldsymbol{\sigma}_3^{nc} \\ \epsilon_{23}^{nc} \\ \epsilon_{13}^{nc} \\ \epsilon_{12}^{nc} \end{Bmatrix} \tag{4}$$

In Eq. 4, v_{nt} is the volume fraction of the CNT with respect to the volume of the RVE of the PMNC (Fig. 4) and $v_p = 1 - v_{nt}$. Also, the superscript nc represents the unwound PMNC material. Substituting Eqs. 1 and 2 into Eqs. 3 and 4, the stress and the strain vectors in the unwound PMNC material can be expressed in terms of the corresponding stress and strain vectors of the constituent phases as follows:

$$\{\boldsymbol{\sigma}^{nc}\} = [C_1]\{\epsilon^{nt}\} + [C_2]\{\epsilon^{p}\} \tag{5}$$

$$\{\epsilon^{nc}\} = [A_1]\{\epsilon^{nt}\} + [A_2]\{\epsilon^{p}\} \tag{6}$$

Also, the relations among the stresses and strains in the CNT and the polymer phase given by (3) can be written as

$$[C_3]\{\epsilon^{nt}\} - [C_4]\{\epsilon^{p}\} = 0 \tag{7}$$

The various matrices appearing in Eqs. 5–7 are given by

$$[C_1] = v_{nt} \begin{bmatrix} 0 & 0 & 0 & 0 & 0 & 0 \\ 0 & 0 & 0 & 0 & 0 & 0 \\ C_{13}^{nt} & C_{23}^{nt} & C_{33}^{nt} & 0 & 0 & 0 \\ 0 & 0 & 0 & 0 & 0 & 0 \\ 0 & 0 & 0 & 0 & 0 & 0 \\ 0 & 0 & 0 & 0 & 0 & 0 \end{bmatrix},$$

$$[C_2] = \begin{bmatrix} C_{11}^{p} & C_{12}^{p} & C_{12}^{p} & 0 & 0 & 0 \\ C_{12}^{p} & C_{11}^{p} & C_{12}^{p} & 0 & 0 & 0 \\ v_p C_{12}^{p} & v_p C_{12}^{p} & v_p C_{11}^{p} & 0 & 0 & 0 \\ 0 & 0 & 0 & C_{44}^{p} & 0 & 0 \\ 0 & 0 & 0 & 0 & C_{44}^{p} & 0 \\ 0 & 0 & 0 & 0 & 0 & C_{44}^{p} \end{bmatrix},$$

$$[C_3] = \begin{bmatrix} C_{11}^{nt} & C_{12}^{nt} & C_{13}^{nt} & 0 & 0 & 0 \\ C_{12}^{nt} & C_{22}^{nt} & C_{23}^{nt} & 0 & 0 & 0 \\ 0 & 0 & 1 & 0 & 0 & 0 \\ 0 & 0 & 0 & C_{44}^{nt} & 0 & 0 \\ 0 & 0 & 0 & 0 & C_{55}^{nt} & 0 \\ 0 & 0 & 0 & 0 & 0 & C_{66}^{nt} \end{bmatrix},$$

$$[C_4] = \begin{bmatrix} C_{11}^p & C_{12}^p & C_{12}^p & 0 & 0 & 0 \\ C_{12}^p & C_{11}^p & C_{12}^p & 0 & 0 & 0 \\ 0 & 0 & 1 & 0 & 0 & 0 \\ 0 & 0 & 0 & C_{44}^p & 0 & 0 \\ 0 & 0 & 0 & 0 & C_{44}^p & 0 \\ 0 & 0 & 0 & 0 & 0 & C_{44}^p \end{bmatrix},$$

$$[V_1] = \begin{bmatrix} v_{nt} & 0 & 0 & 0 & 0 & 0 \\ 0 & v_{nt} & 0 & 0 & 0 & 0 \\ 0 & 0 & 0 & 0 & 0 & 0 \\ 0 & 0 & 0 & v_{nt} & 0 & 0 \\ 0 & 0 & 0 & 0 & v_{nt} & 0 \\ 0 & 0 & 0 & 0 & 0 & v_{nt} \end{bmatrix} \text{ and}$$

$$[V_2] = \begin{bmatrix} v_p & 0 & 0 & 0 & 0 & 0 \\ 0 & v_p & 0 & 0 & 0 & 0 \\ 0 & 0 & 1 & 0 & 0 & 0 \\ 0 & 0 & 0 & v_p & 0 & 0 \\ 0 & 0 & 0 & 0 & v_p & 0 \\ 0 & 0 & 0 & 0 & 0 & v_p \end{bmatrix} \quad (8)$$

Using Eqs. 6 and 7, the local strain vectors $\{\epsilon^{nt}\}$ and $\{\epsilon^{p}\}$ can be expressed in terms of the composite strain $\{\epsilon^{nc}\}$ and subsequently, using them in Eq. 5, the following constitutive relation between the states of stresses and the states of strains at any point in the unwound PMNC material is obtained:

$$\{\sigma^{nc}\} = [C^{nc}]\{\epsilon^{nc}\} \quad (9)$$

where the effective elastic coefficient matrix $[C^{nc}]$ of the lamina of the unwound PMNC is given by

$$[C^{nc}] = [C_1][V_3] + [C_2][V_4] \quad (10)$$

and

$$\begin{aligned} [V_3] &= [V_1] + [V_2][C_4]^{-1}[C_3]; \quad [V_4] \\ &= [V_2] + [V_1][C_3]^{-1}[C_4] \end{aligned} \quad (11)$$

It may be noted that the matrix $[C^{nc}]$ directly provides the effective elastic properties at a point in the portion of the PMNC material surrounding the carbon fiber where the CNT is aligned with the 3-axis of the FFRC. But it is to be noted that with respect to a local material coordinate system 1^0 (2^0, 3^0) as shown in Fig. 3, the matrix $[C^{nc}]$ also provides the effective elastic properties at a point located in the PMNC where the CNT axis (3^0-axis) is oriented at an angle θ with the 3-axis in the 2–3 plane. Thus at any point in the PMNC surrounding the carbon fiber, the location dependent effective elastic coefficient matrix $[\bar{C}^{PMNC}]$ of the PMNC with respect to the 1–2–3 coordinate system can be obtained by the following transformations:

$$[\bar{C}^{PMNC}] = [T_1][C^{nc}][T_1]^{-1} \quad (12)$$

where,

$$[T_1] = \begin{bmatrix} 1 & 0 & 0 & 0 & 0 & 0 \\ 0 & m^2 & n^2 & mn & 0 & 0 \\ 0 & n^2 & m^2 & mn & 0 & 0 \\ 0 & 2mn & 2mn & m^2 & n^2 & 0 & 0 \\ 0 & 0 & 0 & 0 & m & n \\ 0 & 0 & 0 & 0 & n & m \end{bmatrix}$$

with $m = \cos\theta$ and $n = \sin\theta$.

Therefore, the effective elastic properties of the PMNC surrounding the carbon fiber with respect to the principle material coordinate axes of the proposed FFRC varies over an annular cross-section of the PMNC phase of the RVE of the CFF. However, without loss of generality, it may be considered that the volume average of these effective elastic properties $[\bar{C}^{PMNC}]$ over the volume of the PMNC can be treated as the constant effective elastic properties $[C^{PMNC}]$ of the PMNC material surrounding the carbon fiber with respect to the 1–2–3 coordinate axes of the FFRC and is given by

$$[C^{PMNC}] = \frac{1}{\pi(R^2 - a^2)} \int_0^{2\pi} \int_a^R [\bar{C}^{PMNC}]\, r\, dr\, d\theta \quad (13)$$

Thus the effective constitutive relations for the PMNC material with respect to the principle material coordinate axes of the FFRC can be expressed as

$$\{\sigma^{PMNC}\} = [C^{PMNC}]\{\epsilon^{PMNC}\} \quad (14)$$

2.1.2 Effective elastic properties of the CFF

The effective elastic constants of the CFF shown in Fig. 3 may be predicted by estimating the effective elastic properties of a lamina of continuous unidirectional fiber-reinforced composite in which the carbon fiber is the reinforcement and the matrix phase is the PMNC material whose effective elastic properties are given by Eq. 13. The cross sections of the RVE of such lamina have been illustrated in Fig. 5a. Here, the length of the carbon fiber aligns with the 1-direction. The MOM approach derived in the previous section is augmented to estimate the effective elastic properties of the CFF. Similar to Eqs. 3 and 4, the iso-field conditions and the rules of mixture for the RVE shown in Fig. 5a can be written as

$$\begin{Bmatrix} \epsilon_1^f \\ \sigma_2^f \\ \sigma_3^f \\ \sigma_{23}^f \\ \sigma_{13}^f \\ \sigma_{12}^f \end{Bmatrix} = \begin{Bmatrix} \epsilon_1^{PMNC} \\ \sigma_2^{PMNC} \\ \sigma_3^{PMNC} \\ \sigma_{23}^{PMNC} \\ \sigma_{13}^{PMNC} \\ \sigma_{12}^{PMNC} \end{Bmatrix} = \begin{Bmatrix} \epsilon_1^{CFF} \\ \sigma_2^{CFF} \\ \sigma_3^{CFF} \\ \sigma_{23}^{CFF} \\ \sigma_{13}^{CFF} \\ \sigma_{12}^{CFF} \end{Bmatrix} \quad (15)$$

and

$$\bar{v}_f \begin{Bmatrix} \sigma_1^f \\ \epsilon_2^f \\ \epsilon_3^f \\ \epsilon_{23}^f \\ \epsilon_{13}^f \\ \epsilon_{12}^f \end{Bmatrix} + v_{PMNC} \begin{Bmatrix} \sigma_1^{PMNC} \\ \epsilon_2^{PMNC} \\ \epsilon_3^{PMNC} \\ \epsilon_{23}^{PMNC} \\ \epsilon_{13}^{PMNC} \\ \epsilon_{12}^{PMNC} \end{Bmatrix} = \begin{Bmatrix} \sigma_1^{CFF} \\ \epsilon_2^{CFF} \\ \epsilon_3^{CFF} \\ \epsilon_{23}^{CFF} \\ \epsilon_{13}^{CFF} \\ \epsilon_{12}^{CFF} \end{Bmatrix} \quad (16)$$

In Eq. 16, $\bar{v}_f$ and $\bar{v}_P$ are the volume fraction of the carbon fiber and the PMNC material, respectively, with respect to the volume of the RVE of the CFF. Using Eqs. 14–16, and following the procedure for deriving Eq. 10, the constitutive relations of the CFF can be obtained as follows:

$$\{\sigma^{CFF}\} = [C^{CFF}]\{\epsilon^{CFF}\} \quad (17)$$

in which the effective elastic coefficient matrix $[C^{CFF}]$ of the CFF is given by

$$[C^{CFF}] = [C_5 W_7^{-1} + C_6 W_8^{-1}] \quad (18)$$

The various matrices appearing in Eq. 18 are

$$C_6 = \begin{bmatrix} v_{PMNC} C_{11}^{PMNC} & v_{PMNC} C_{12}^{PMNC} & v_{PMNC} C_{13}^{PMNC} & 0 & 0 & 0 \\ C_{12}^{PMNC} & C_{22}^{PMNC} & C_{23}^{PMNC} & 0 & 0 & 0 \\ C_{13}^{PMNC} & C_{23}^{PMNC} & C_{33}^{PMNC} & 0 & 0 & 0 \\ 0 & 0 & 0 & C_{44}^{PMNC} & 0 & 0 \\ 0 & 0 & 0 & 0 & C_{55}^{PMNC} & 0 \\ 0 & 0 & 0 & 0 & 0 & C_{66}^{PMNC} \end{bmatrix},$$

$$C_5 = \bar{v}_f \begin{bmatrix} C_{11}^f & C_{12}^f & C_{13}^f & 0 & 0 & 0 \\ 0 & 0 & 0 & 0 & 0 & 0 \\ 0 & 0 & 0 & 0 & 0 & 0 \\ 0 & 0 & 0 & 0 & 0 & 0 \\ 0 & 0 & 0 & 0 & 0 & 0 \\ 0 & 0 & 0 & 0 & 0 & 0 \end{bmatrix}, \quad C_7 = \begin{bmatrix} 1 & 0 & 0 & 0 & 0 & 0 \\ C_{12}^f & C_{22}^f & C_{23}^f & 0 & 0 & 0 \\ C_{13}^f & C_{23}^f & C_{33}^f & 0 & 0 & 0 \\ 0 & 0 & 0 & C_{44}^f & 0 & 0 \\ 0 & 0 & 0 & 0 & C_{55}^f & 0 \\ 0 & 0 & 0 & 0 & 0 & C_{66}^f \end{bmatrix},$$

$$C_8 = \begin{bmatrix} 1 & 0 & 0 & 0 & 0 & 0 \\ C_{12}^{PMNC} & C_{22}^{PMNC} & C_{23}^{PMNC} & 0 & 0 & 0 \\ C_{13}^{PMNC} & C_{23}^{PMNC} & C_{33}^{PMNC} & 0 & 0 & 0 \\ 0 & 0 & 0 & C_{44}^{PMNC} & 0 & 0 \\ 0 & 0 & 0 & 0 & C_{55}^{PMNC} & 0 \\ 0 & 0 & 0 & 0 & 0 & C_{66}^{PMNC} \end{bmatrix}, \quad W_5 = \begin{bmatrix} 0 & 0 & 0 & 0 & 0 & 0 \\ 0 & \bar{v}_f & 0 & 0 & 0 & 0 \\ 0 & 0 & \bar{v}_f & 0 & 0 & 0 \\ 0 & 0 & 0 & \bar{v}_f & 0 & 0 \\ 0 & 0 & 0 & 0 & \bar{v}_f & 0 \\ 0 & 0 & 0 & 0 & 0 & \bar{v}_f \end{bmatrix}, \quad (19)$$

$$W_6 = \begin{bmatrix} 1 & 0 & 0 & 0 & 0 & 0 \\ 0 & v_{PMNC} & 0 & 0 & 0 & 0 \\ 0 & 0 & v_{PMNC} & 0 & 0 & 0 \\ 0 & 0 & 0 & v_{PMNC} & 0 & 0 \\ 0 & 0 & 0 & 0 & v_{PMNC} & 0 \\ 0 & 0 & 0 & 0 & 0 & v_{PMNC} \end{bmatrix},$$

$W_7 = W_5 + W_6 C_8^{-1} C_7$ and $W_8 = W_6 + W_5 C_7 C_8^{-1}$

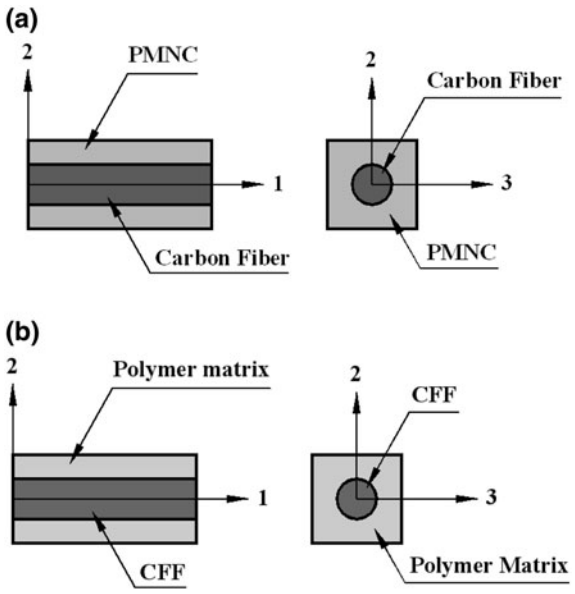

Fig. 5 a Cross sections of the RVE of the CFF. b Cross sections of the RVE of the FFRC

2.1.3 Effective elastic properties of the FFRC

It may be reiterated that the RVE of the FFRC lamina can be viewed as being comprised of the CFF and the monolithic polymer matrix. The cross sections of such an RVE (Meguid and Zhu 1995) are shown in Fig. 5b. In order to satisfy the perfectly bonding situation between the CFF and the polymer, the iso-field conditions and the rules of mixture appropriate for this RVE are given by

$$\begin{Bmatrix} \epsilon_1^{CFF} \\ \sigma_2^{CFF} \\ \sigma_3^{CFF} \\ \sigma_{23}^{CFF} \\ \sigma_{13}^{CFF} \\ \sigma_{12}^{CFF} \end{Bmatrix} = \begin{Bmatrix} \epsilon_1^{p} \\ \sigma_2^{p} \\ \sigma_3^{p} \\ \sigma_{23}^{p} \\ \sigma_{13}^{p} \\ \sigma_{12}^{p} \end{Bmatrix} = \begin{Bmatrix} \epsilon_1 \\ \sigma_2 \\ \sigma_3 \\ \sigma_{23} \\ \sigma_{13} \\ \sigma_{12} \end{Bmatrix} \quad (20)$$

and

$$v_{CFF} \begin{Bmatrix} \sigma_1^{CFF} \\ \epsilon_2^{CFF} \\ \epsilon_3^{CFF} \\ \epsilon_{23}^{CFF} \\ \epsilon_{13}^{CFF} \\ \epsilon_{12}^{CFF} \end{Bmatrix} + \bar{v}_p \begin{Bmatrix} \sigma_1^{p} \\ \epsilon_2^{p} \\ \epsilon_3^{p} \\ \epsilon_{23}^{p} \\ \epsilon_{13}^{p} \\ \epsilon_{12}^{p} \end{Bmatrix} = \begin{Bmatrix} \sigma_1 \\ \epsilon_2 \\ \epsilon_3 \\ \epsilon_{23} \\ \epsilon_{13} \\ \epsilon_{12} \end{Bmatrix} \quad (21)$$

In Eq. 21, v_{CFF} and $\bar{v}_P$ are the volume fractions of the CFF and the polymer matrix, respectively, with respect to the FFRC. It may be noted that unlike the constituent phases, the symbols denoting the states of stresses and strains in the FFRC are written without using the superscript. Using Eqs. 17, 20 and 21, the strains in the constitutive phases can be expressed in terms of the strains in the proposed homogenous FFRC and the constitutive relations for the proposed FFRC are derived as follows:

$$\{\sigma\} = [C]\{\epsilon\} \quad (22)$$

where the effective elastic coefficient matrix $[C]$ of the FFRC is given by

$$[C] = [C_9][T_{11}]\left([I] + [C_{10}][T_{12}]\right)^{-1} \quad (23)$$

with

$$[T_{11}] = [T_9] + [T_{10}][C_{12}]^{-1}[C_{11}] \text{ and}$$

$$[T_{12}] = [T_{10}] + [T_9][C_{11}]^{-1}[C_{12}]$$

$$[T_9] = \begin{bmatrix} 0 & 0 & 0 & 0 & 0 & 0 \\ 0 & v_{CFF} & 0 & 0 & 0 & 0 \\ 0 & 0 & v_{CFF} & 0 & 0 & 0 \\ 0 & 0 & 0 & v_{CFF} & 0 & 0 \\ 0 & 0 & 0 & 0 & v_{CFF} & 0 \\ 0 & 0 & 0 & 0 & 0 & v_{CFF} \end{bmatrix},$$

$$[T_{10}] = \begin{bmatrix} 1 & 0 & 0 & 0 & 0 & 0 \\ 0 & \bar{v}_P & 0 & 0 & 0 & 0 \\ 0 & 0 & \bar{v}_P & 0 & 0 & 0 \\ 0 & 0 & 0 & \bar{v}_P & 0 & 0 \\ 0 & 0 & 0 & 0 & \bar{v}_P & 0 \\ 0 & 0 & 0 & 0 & 0 & \bar{v}_P \end{bmatrix},$$

$$[C_{11}] = \begin{bmatrix} 1 & 0 & 0 & 0 & 0 & 0 \\ C_{12}^{CFF} & C_{22}^{CFF} & C_{23}^{CFF} & 0 & 0 & 0 \\ C_{13}^{CFF} & C_{23}^{CFF} & C_{33}^{CFF} & 0 & 0 & 0 \\ 0 & 0 & 0 & C_{44}^{CFF} & 0 & 0 \\ 0 & 0 & 0 & 0 & C_{55}^{CFF} & 0 \\ 0 & 0 & 0 & 0 & 0 & C_{66}^{CFF} \end{bmatrix},$$

$$[C_{12}] = \begin{bmatrix} 1 & 0 & 0 & 0 & 0 & 0 \\ C_{12}^{p} & C_{11}^{p} & C_{12}^{p} & 0 & 0 & 0 \\ C_{12}^{p} & C_{12}^{p} & C_{11}^{p} & 0 & 0 & 0 \\ 0 & 0 & 0 & C_{44}^{p} & 0 & 0 \\ 0 & 0 & 0 & 0 & C_{44}^{p} & 0 \\ 0 & 0 & 0 & 0 & 0 & C_{44}^{p} \end{bmatrix},$$

$$[C_9] = [C_{CFF}] \begin{bmatrix} C_{11}^{CFF} & C_{12}^{CFF} & C_{13}^{CFF} & 0 & 0 & 0 \\ 0 & 0 & 0 & 0 & 0 & 0 \\ 0 & 0 & 0 & 0 & 0 & 0 \\ 0 & 0 & 0 & 0 & 0 & 0 \\ 0 & 0 & 0 & 0 & 0 & 0 \\ 0 & 0 & 0 & 0 & 0 & 0 \end{bmatrix},$$

$$[C_{10}] = \begin{bmatrix} \nu_P C_{11}^p & \nu_P C_{12}^p & \nu_P C_{12}^p & 0 & 0 & 0 \\ C_{12}^p & C_{11}^p & C_{12}^p & 0 & 0 & 0 \\ C_{12}^p & C_{12}^p & C_{11}^p & 0 & 0 & 0 \\ 0 & 0 & 0 & C_{44}^p & 0 & 0 \\ 0 & 0 & 0 & 0 & C_{44}^p & 0 \\ 0 & 0 & 0 & 0 & 0 & C_{44}^p \end{bmatrix}. \quad (24)$$

2.2 Mori–Tanaka (MT) method

The previous micromechanics model is based on the assumptions and the rules of mixture delineated by Eqs. 3 and 4, respectively, which imply the perfect bonding condition between the CNT fiber and the matrix. However, it is imperative to justify the validity of these assumption and the rules of mixture for modeling the perfect bonding conditions of the MOM approach. For this purpose, another micromechanics model based on the Mori–Tanaka (MT) method which does not require to satisfy Eqs. 3 and 4 will be presented here. Although it is mentioned in the previous section that the weakened interface or the interphase between the CNT fiber and the polymer matrix does not affect the effective elastic properties to a considerable extent (Esteva and Spanos 2009; Tsai et al. 2010), we intend to investigate the effect of the interphase between the CNT and the polymer on the effective properties of this FFRC employing the MT method. The non bonded van der Waals interaction between an atom of CNT and an atom of the polymer is characterized here by introducing an interphase (Odegard et al. 2003; Tsai et al. 2010). The effective properties of such interphase resembling a solid continuum can be determined by molecular dynamics simulation and are readily available in the open literature (Tsai et al. 2010). Thus considering this interphase between a CNT and the polymer matrix, the micromechanical model of the unwound PMNC by the MT method will be a three-phase MT model. Utilizing the effective properties of the interphase, the CNT properties, the polymer matrix properties and the procedure of the MT method for multiple inclusions (Dunn and Ledbetter 1995), a three-phase MT model can be derived to estimate the effective elastic coefficient matrix of the unwound PMNC. The explicit formulation of such three-phase MT model can be derived as

$$[C^{nc}] = [C^p] + \left[\left(v_{nt} + v_i \right) \left([C^i] - [C^p] \right) [A_V] + v_{nt} \left([C^{nt}] - [C^i] \right) [A_{nt}] \right] \left[v_p [I] + \left(v_{nt} + v_i \right) [A_V] \right]^{-1} \quad (25)$$

where $[C^p]$ and v_i represent the linear elastic coefficient matrix and the volume fraction of the interphase, respectively, while V denotes the domain comprising a CNT and the interphase surrounding this CNT. The concentration tensors $[A_V]$ and $[A_{nt}]$ appearing in Eq. 25 are given by

$$[A_V] = [I] + [S_V][\Phi_V] \text{ and } [A_{nt}] = [I] + [A_S][S_{nt}][\Phi_{nt}] \quad (26)$$

The various matrices appearing in (26) are

$$[\Phi_{nt}] = \left[\left([S_{nt}] - [C^2]^{-1} + [A_S] \right) \left([S_{nt}] - \frac{v_{nt}}{v_i} [A_S] + [C^2]^{-1} \right)^{-1} \left([S_{nt}] - \frac{v_{nt}}{v_i} [A_S] + [C^1]^{-1} \right) \right]^{-1},$$

$$[\Phi_i] = \left[[A_S] + \left([S_{nt}] - [C^2]^{-1} + \left([S_{nt}] - \frac{v_{nt}}{v_i} [A_S] + [C^1]^{-1} \right)^{-1} \left([S_{nt}] - \frac{v_{nt}}{v_i} [A_S] + [C^2]^{-1} \right) \right]^{-1},$$

$$[\Phi_V] = \frac{v_{nt}}{v_{nt} + v_i} [\Phi_{nt}] + \frac{v_i}{v_{nt} + v_i} [\Phi_i],$$

$$[A_S] = [S_{nt}] - [S_V], \left[C^1 \right] = \left([C^{nt}] - [C^p] \right)^{-1} [C^p] + [I] \text{ and } \left[C^2 \right] = \left([C^i] - [C^p] \right)^{-1} [C^p] + [I]. \quad (27)$$

Also, in the above matrices $[S_V]$ and $[S_{nt}]$ indicate the Eshelby's tensor for the domains V and nt, respectively, and $[I]$ is an identity matrix. As assumed in the previous model, the CNT may be treated as a

solid circular cylindrical fiber (Gao and Li 2005; Tsai et al. 2010). Thus the specific form of the Eshelby tensor for cylindrical inclusion given by Qui and Weng (1990) is utilized to compute the matrices S_V [and S_{nt}]. Once C^{nc} is computed from Eq. 25, Eqs. 12 and 13 are used to estimate the average effective elastic coefficient matrix $[C^{PMNC}]$ of the PMNC material surrounding the carbon fiber. Note that if the perfectly bonding condition between a CNT and the polymer is assumed the conventional two-phase MT method (Mori and Tanaka 1973) is used to predict the effective coefficient matrix C^{nc} of the unwound PMNC.

The effective elastic properties of the CFF can be predicted by estimating the effective elastic properties of a composite in which the carbon fiber is the reinforcement and the matrix phase is the PMNC material. Thus according to the two-phase model by the MT method (Mori and Tanaka 1973), the effective elastic coefficient matrix for the CFF is given by

$$[C^{CFF}] = [C^{PMNC}] + \bar{v}_f([C^f] - [C^{PMNC}])A_1 \quad (28)$$

in which the matrix of the strain concentration factors are as follows

$$A_1 = [\tilde{A}_1][v_{PMNC} I + \bar{v}_f[\tilde{A}_1]]^{-1};$$
$$[\tilde{A}_1] = \left[I + S_1 ([C^{PMNC}])^{-1}([C^f] - [C^{PMNC}])\right]^{-1}$$

where, the Eshelby's tensor S_1 is computed based on the properties of the PMNC matrix and the shape of the carbon fiber. It is worthwhile to note that the PMNC matrix is transversely isotropic and consequently, the Eshelby tensor (Jiang and Martin 1998) corresponding to transversely isotropic material is utilized for computing S_1 while the inclusion is a circular cylindrical fiber.

Finally, considering the CFF as the cylindrical inclusion embedded in the isotropic polymer matrix the effective elastic properties C of the FFRC can be derived by the two-phase MT method (Mori and Tanaka 1973) as follows:

$$C = C^p + v_{CFF}([C^{CFF}] - C^p)A_2 \quad (29)$$

in which the matrix of the strain concentration factors are given by

$$A_2 = [\tilde{A}_2][v_P I + v_{CFF}[\tilde{A}_2]]^{-1} \quad \text{and}$$
$$[\tilde{A}_2] = \left[I + S_2 (C^p)^{-1}([C^{CFF}] - C^p)\right]^{-1}$$

3 Results and Discussion

In this section, numerical values of the effective elastic properties of the proposed FFRC are evaluated using the two different models derived in the preceding sections. Zig-zag single-walled CNTs, the carbon fiber and the polyimide polymer matrix are used for evaluating the numerical results. Their material properties are listed in Table 1. The effective properties and the thickness of the hollow circular cylindrical continuum representing the interphase between a CNT and the polyimide matrix are also presented in Table 1. Unless otherwise mentioned, (10, 0) CNT is used for plotting the results and the value of the diameter of the carbon fiber is assumed as $2a = 10\ \mu m$. Volume fraction of CNTs

Table 1 Material properties of the constituent phases of FFRC

Material	Ref.	C_{11} (GPa)	C_{12} (GPa)	C_{13} (GPa)	C_{23} (GPa)	C_{33} (GPa)	C_{44} (GPa)	C_{66} (GPa)	(nm)
(10, 0) CNT	(Tsai et al. 2010)	709.9	172.4	240	240	1513.1	1120	268.7	$d_n = 0.78$
Interphase		29.6	15.2	15.2	15.2	29.6	7.2	7.2	$G_{ap} = 0.3333$
(14, 0) CNT	(Tsai et al. 2010)	557.5	137.5	187.7	187.7	1082.8	779.2	210	$d_n = 1.1$
Interphase		27.63	14.23	14.23	14.23	27.63	6.70	6.70	$G_{ap} = 0.3236$
(18, 0) CNT	(Tsai et al. 2010)	472.9	118.7	159.7	159.7	846.1	596.3	177.1	$d_n = 1.42$
Interphase		27.55	14.19	14.19	14.19	27.55	6.68	6.68	$G_{ap} = 0.3158$
Carbon fiber	(Honjo 2007)	236.4	10.6	10.6	10.7	24.8	7	25	$d = 10000$
Polyimide	(Odegard et al. 2005)	9	6	6	6	9	1.5	1.5	–

(v_{CNT}) in the FFRC depends on the CNT diameter, the carbon fiber diameter and the surface to surface distance of two adjacent radially aligned CNTs at their roots. If there are no other phases or materials in between CNTs, it is reported (Jiang et al. 2009) that the minimum surface to surface distance between two adjacent CNTs is the equilibrium van der Waals distance, which is about 0.34 nm. Since in the PMNC material, polyimide polymer molecules fill the gap between CNTs and the formation of the interphase is also considered, the surface to surface distance between the two adjacent CNTs at their roots is considered as 1.7 nm. Recall that the FFRC lamina can be viewed as being comprised of the CFFs and the polyimide matrix. For fibers with circular cross section, it is well known that hexagonal array of packing is the optimal packing of fibers and the corresponding maximum fiber volume fraction is 0.9069. Hence, in the proposed FFRC, the hexagonal packing array of CFFs is considered as shown in Fig. 6 for evaluating the numerical results. It is also assumed that the radially grown CNTs are uniformly spaced on the surface of the carbon fiber. Note that although the volume fraction of CFF is 0.9069, the volume fraction of carbon fiber is much less than 0.9069.

The determination of v_{CNT} in the FFRC is an important issue. It is obvious that the constructional feature of the FFRC put a constraint on the maximum value of v_{CNT}. Based on the surface to surface distance at the roots of two adjacent CNTs and the CNT diameter, the maximum number of CNTs grown on the surface of a carbon fiber of particular diameter can be determined. Then based on the carbon fiber volume fraction (v_f) in the FFRC, the maximum value of v_{CNT} can be determined as

$$(v_{CNT})_{max} = \frac{\pi d_n^2}{2(d_n + 1.7)^2}\left(\sqrt{\frac{\pi v_f}{2\sqrt{3}}} - v_f\right) \quad (30)$$

where d_n is the diameter of the CNT. The derivation of Eq. 30 has been presented in the section of "Appendix". It is evident from Eq. 30 that when $v_f = 0$, v_{CNT} is zero. Also, when $v_f = \pi/2\sqrt{3}$ i.e., there is no PMNC, the value of v_{CNT} is zero. Thus the maximum value of v_{CNT} given by Eq. 30 will be maximum at a particular value of the v_f. Figure 7 illustrates the variation of the maximum value of the CNT volume fraction in the FFRC (v_{CNT}) with the carbon fiber volume fraction (v_f) while the values of v_f varies from 0.1 to $\pi/2\sqrt{3}$. It may be observed from this figure that the maximum values of v_{CNT} for different CNT diameters are almost independent of the CNT diameter and are maximized at $v_f = 0.24$. Also, it may be noted that if v_f increases then either the diameter or the number of the carbon fiber increases. This results in the reduction of the length of the CNTs which in turn causes decrease in the volume of the CNTs in the CFF and the FFRC beyond a value of v_f as 0.24. In what follows, unless otherwise mentioned the effective properties of the FFRC are computed for a particular value of v_f while the maximum value of v_{CNT} corresponding to this value of v_f is considered for the computation. First, the effective elastic properties of the PMNC surrounding the carbon fiber computed by the models

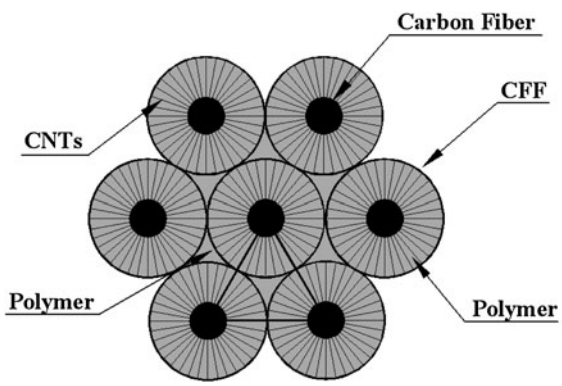

Fig. 6 Hexagonal packing array comprised of CFFs

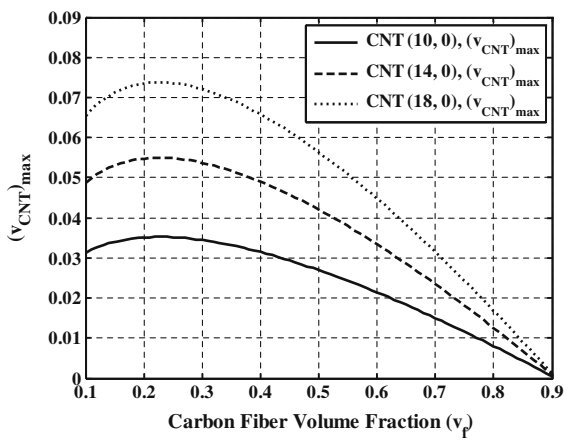

Fig. 7 Variation of the maximum CNT volume fraction with the carbon fiber volume fraction in the FFRC

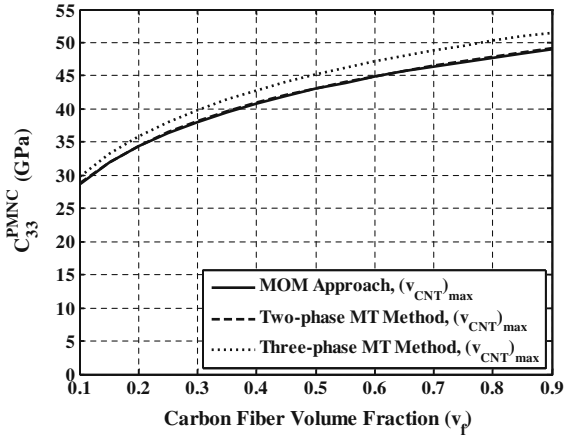

Fig. 8 Variation of the effective elastic coefficient C_{33}^{PMNC} of the PMNC with the carbon fiber volume fraction

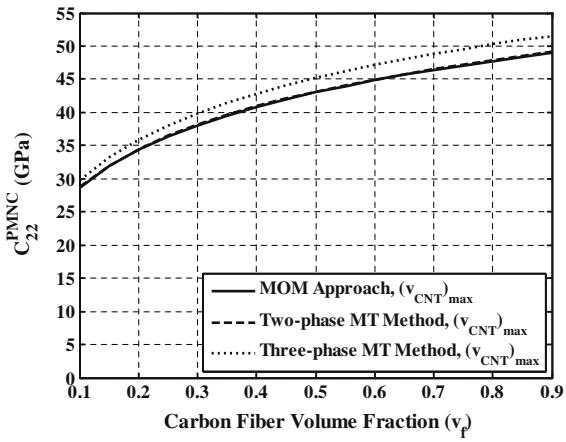

Fig. 9 Variation of the effective elastic coefficient C_{22}^{PMNC} of the PMNC with the carbon fiber volume fraction

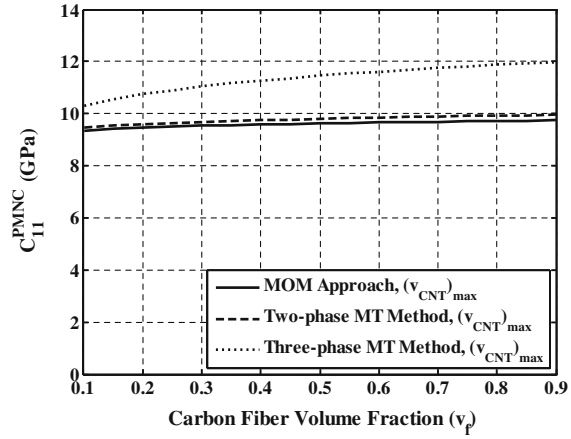

Fig. 10 Variation of the effective elastic coefficient C_{11}^{PMNC} of the PMNC with the carbon fiber volume fraction

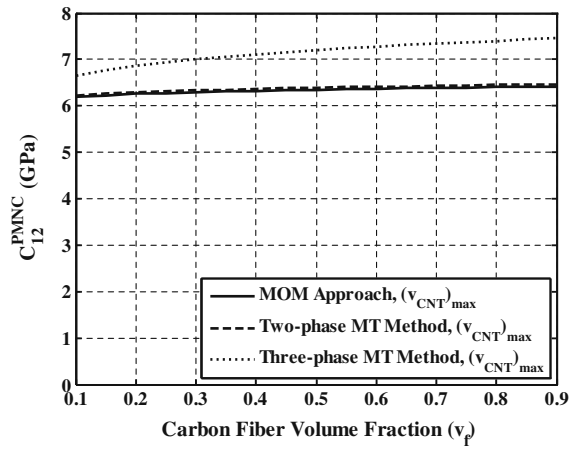

Fig. 11 Variation of the effective elastic coefficient C_{12}^{PMNC} of the PMNC with the carbon fiber volume fraction

derived in the previous sections are illustrated in Figs. 8, 9, 10, 11, 12, and 13. It should be noted that the models by the MOM approach and the two-phase MT method estimate the properties with the assumption of perfect bonding condition between CNT and the matrix (i.e., without the interphase). On the other hand, the model by the three-phase MT method predicts the properties in the presence of the interphase. Figure 8 illustrates the variation of the effective elastic coefficient C_{33}^{PMNC} of the PMNC with the carbon fiber volume fraction (v_f). It can be observed that the models by the MOM approach and the two-phase MT method, predict identical estimates for C_{33}^{PMNC} while the three-phase MT method marginally overestimates the value of C_{33}^{PMNC}. It may be mentioned that the previous researchers (Esteva and Spanos 2009; Tsai et al. 2010) also reported the similar trend of results for estimating the effective longitudinal properties of CNT-reinforced composite. The constructional feature of the PMNC reveals that the PMNC would be a transversely isotropic material. This is corroborated by the prediction of C_{22}^{PMNC} which is identical to that of C_{33}^{PMNC} as shown in Fig. 9. Figure 10 illustrates the variation of the effective transverse elastic coefficient C_{11}^{PMNC} of the PMNC with the carbon fiber volume fraction (v_f). It may be observed that the three-phase MT method provides slightly enhanced estimate for the value of

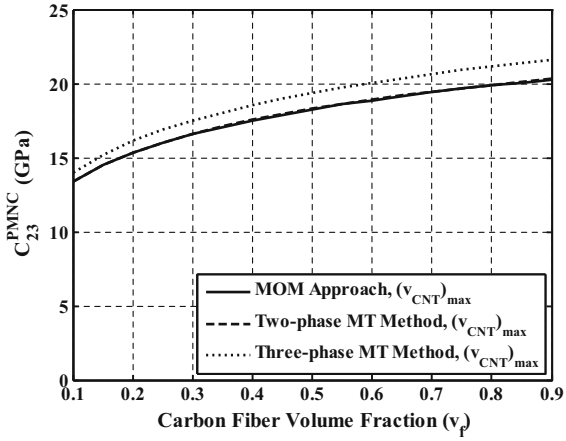

Fig. 12 Variation of the effective elastic coefficient C_{23}^{PMNC} of the PMNC with the carbon fiber volume fraction

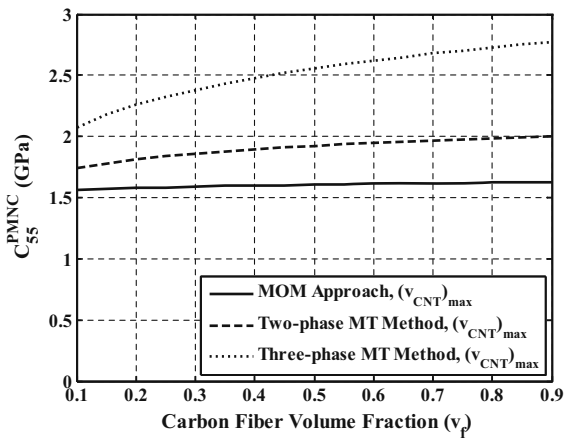

Fig. 13 Variation of the effective elastic coefficient C_{55}^{PMNC} of the PMNC with the carbon fiber volume fraction

C_{11}^{PMNC} as compared to that predicted by the MOM approach and the two-phase MT method. This result is also coherent with the previously reported results (Esteva and Spanos 2009, Tsai et al. 2010). Similar predictions have also been obtained for the effective elastic coefficient C_{12}^{PMNC} as shown in Fig. 11. Figure 12 demonstrates the variation of the effective elastic coefficient C_{23}^{PMNC} of the PMNC with the carbon fiber volume fraction (v_f). In this case also, the two-phase micromechanical methods predict almost identical estimates for C_{23}^{PMNC} and the three-phase MT method slightly overestimates the value of C_{23}^{PMNC}. The three-phase MT method overestimates the effective value of C_{55}^{PMNC} as compared to the

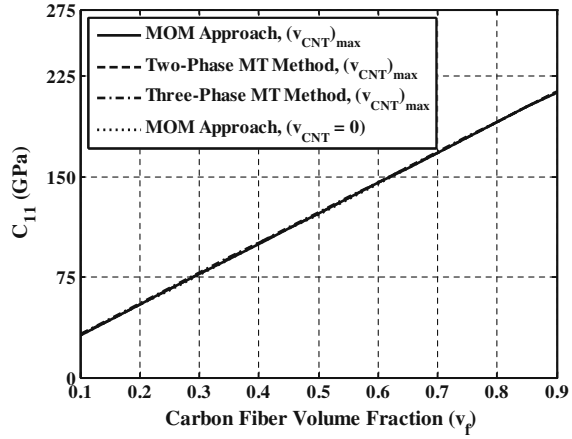

Fig. 14 Variation of the effective elastic coefficient C_{11} of the FFRC with the carbon fiber volume fraction

two-phase models as shown in Fig. 13. Almost 100% agreement between the two sets of the effective properties estimated by the MOM approach and the two-phase MT method, respectively as shown in Figs. 8, 9, 10, 11, 12, and 13, ensures the validity of the assumptions and the rules of mixture for deriving the model using the MOM approach. Next, the estimated effective properties of the PMNC are used to compute the effective properties of the CFF and the FFRC. However, for the sake of brevity, effective properties of the CFF are not presented here. Figure 14 illustrates the variation of the effective elastic coefficient C_{11} of the proposed FFRC with the carbon fiber volume fraction (v_f). It may be observed that all the methods predict identical estimates for C_{11} of the FFRC. It is important to note from this figure that the radial growing of aligned CNTs on the surface of the carbon fibers does not affect the magnitude of the effective in-plane elastic coefficient C_{11} when compared with that of the elastic coefficient C_{11} without CNTs. This may be attributed to the fact that the CNTs are grown transverse to the carbon fiber, the elastic properties of CNT transverse to its axis (i.e., along 1-direction) are much less than those along its axis and the CNT volume fraction is low. It is also important to be note from Fig. 14 that although the interphase between the CNT and the polyimide matrix locally affects the value of the elastic coefficient C_{11}^{PMNC} of the PMNC material (Fig. 10), it does not influence the effective value of the elastic coefficient C_{11} of the FFRC. Figure 15 illustrates the variation of the effective transverse

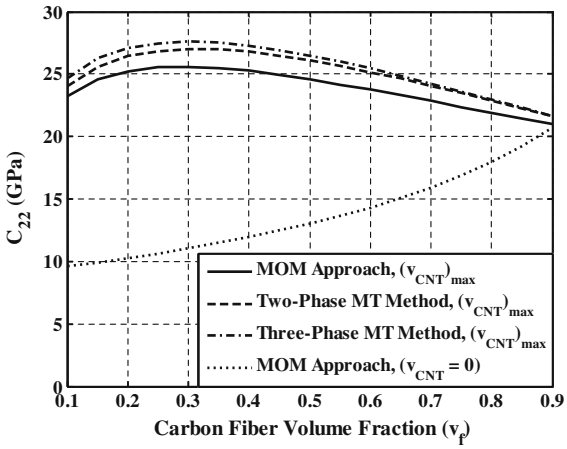

Fig. 15 Variation of the effective elastic coefficient C_{22} of the FFRC with the carbon fiber volume fraction

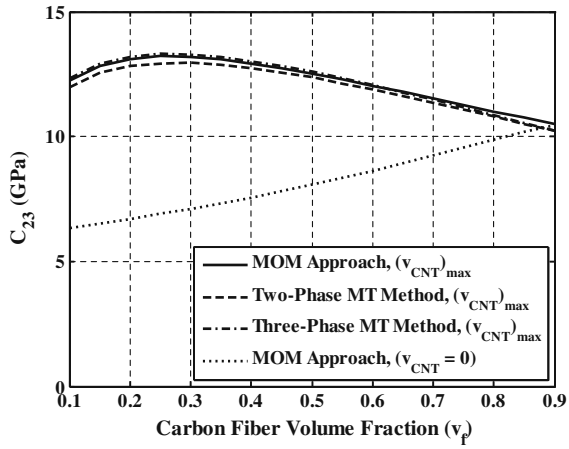

Fig. 16 Variation of the effective elastic coefficient C_{23} of the FFRC with the carbon fiber volume fraction

elastic coefficient C_{22} of the proposed FFRC with the carbon fiber volume fraction (v_f). It may be noted that for $v_{CNT} \neq 0$, the three-phase MT method marginally overestimates the value of C_{22} as compared to the two-phase MT model. But, it may be importantly observed from Fig. 15 that even if the interphase is not considered, the effective value of C_{22} of the proposed FFRC is significantly larger than that of the composite without CNTs. This is attributed to the fact that the radially grown CNTs enhance the out-of-plane stiffness of the matrix surrounding the carbon fibers while the transverse properties are matrix dominant properties. Since the FFRC is transversely isotropic with 1-axis as the axis of symmetry, the values of the effective elastic coefficients C_{33} of the FFRC are found to be identical to those of C_{22} and for brevity are not presented here. Radially grown CNTs also significantly improve the values of the effective elastic coefficient C_{23} of the FFRC as shown in Fig. 16. But the interphase does not influence this constant. It may be observed from Fig. 17 that the growing of CNTs on the surface of the carbon fiber moderately improves the value of the elastic coefficient C_{12} of the FFRC. Since the FFRC is transversely isotropic, similar results are also obtained for the effective elastic coefficient C_{13}. Figure 18 depicts the variation of the effective elastic coefficient C_{55} of the proposed FFRC with the carbon fiber volume fraction. It may be observed that both the MT methods overestimates this constant as compared to MOM approach for $v_{CNT} \neq 0$. Identical results are also predicted for C_{66} but not shown here. Comparison of

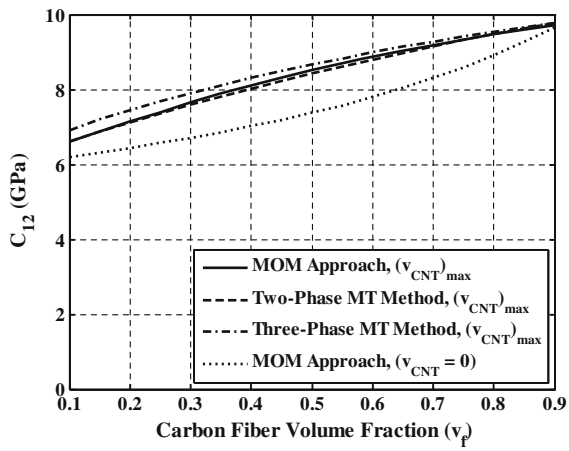

Fig. 17 Variation of the effective elastic coefficient C_{12} of the FFRC with the carbon fiber volume fraction

the model by the MOM approach with that by the MT methods reveals that the MOM approach yields conservative estimates of the elastic constants of the proposed FFRC. Hence, predictions by the MOM approach have been considered in the subsequent results for investigating the effect of the CNT diameter and the maximum CNT volume fraction on the effective properties of the FFRC.

Figures 19, 20, 21 illustrate the comparisons of the effective elastic constants of the proposed FFRC for different values of the CNT diameter. It may be mentioned that as the integer for designating the zig-zag type CNT increases, the diameter of the CNT increases. Figure 19 illustrates that the CNT diameter does not influence the effective elastic coefficient C_{11}

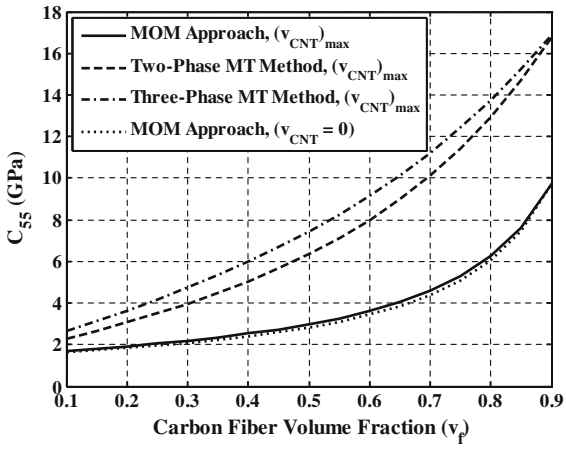

Fig. 18 Variation of the effective elastic coefficient C_{55} of the FFRC with the carbon fiber volume fraction

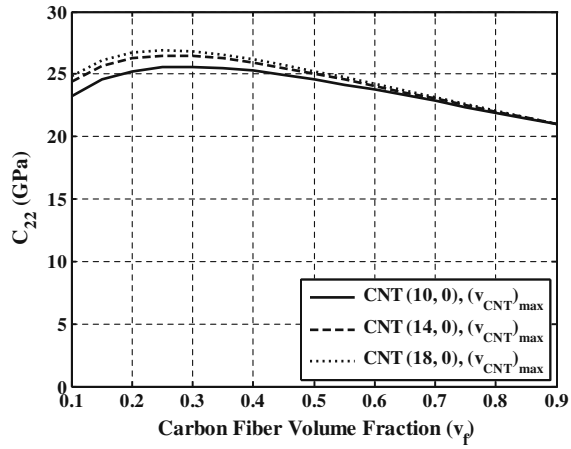

Fig. 20 Variation of the effective elastic coefficient C_{22} of the FFRC with the carbon fiber volume fraction

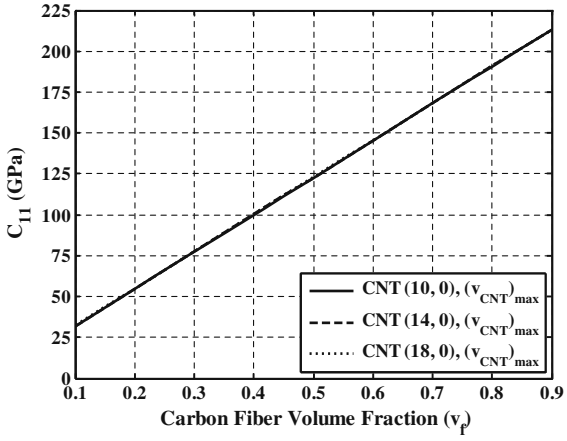

Fig. 19 Variation of the effective elastic coefficient C_{11} of the FFRC with the carbon fiber volume fraction

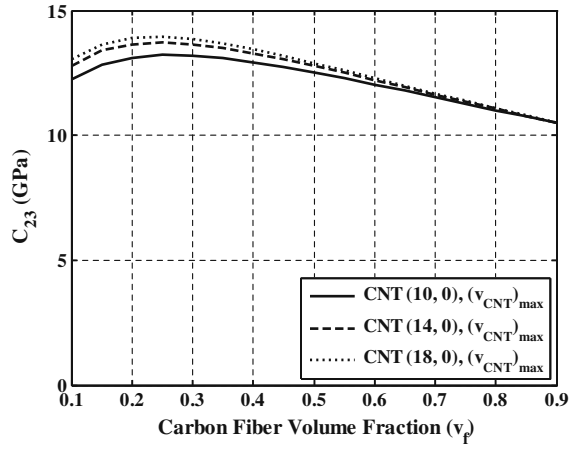

Fig. 21 Variation of the effective elastic coefficient C_{23} of the FFRC with the carbon fiber volume fraction

of the proposed FFRC. Figure 20 reveals that the increase in the CNT diameter marginally increases the value of the effective elastic coefficient C_{22} of the FFRC for low carbon fiber volume fraction. The same is true for the effective elastic coefficient C_{23} as depicted in Fig. 21. This may be attributed to the fact that as the diameter of the CNT increases, the value of the CNT volume fraction increases as shown in Fig. 7 which results in the increase in the values of the effective elastic constants of the FRVMNC. Similar predictions for the other effective elastic coefficients have also been obtained, but for the sake of brevity they are not presented here. So far, the effect of radial growing of CNTs on the surface of the carbon fiber has been studied by considering the maximum value of the CNT volume fraction for a particular value of v_f. However, the variation of the CNT volume fraction for a particular value of v_f would be an important study. For this the discrete values of the carbon fiber volume fraction are considered as 0.2, 0.3, 0.4 and 0.5. The maximum values of v_{CNT} corresponding to these values of v_f are 0.0735, 0.0721, 0.0658 and 0.0564, respectively. However, for presenting the results, the limiting value of v_{CNT} has been considered as 0.0564. Once again, Fig. 22 illustrates that the effective value of C_{11} of the proposed FFRC is independent of the variation of the CNT volume fraction. Figure 23 depicts the variation of the effective elastic coefficient C_{22} of the FFRC with the CNT volume fraction. It may be observed

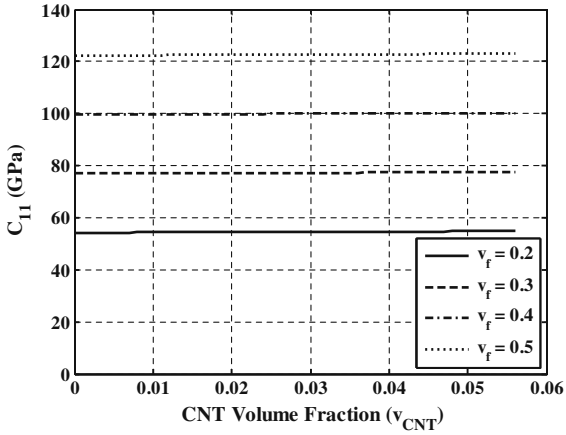

Fig. 22 Variation of the effective elastic coefficient C_{11} of the FFRC with the CNT volume fraction ((18, 0) CNT)

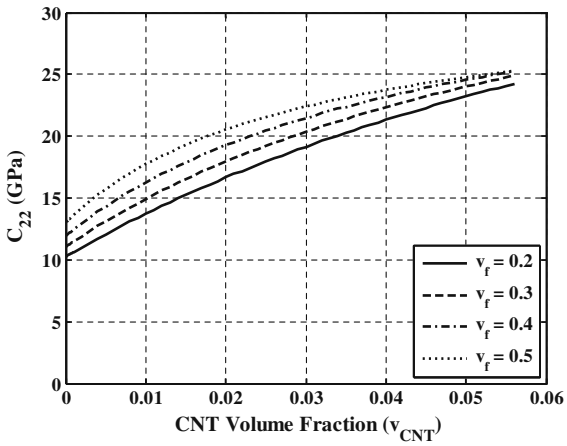

Fig. 23 Variation of the effective elastic coefficient C_{22} of the FFRC with the CNT volume fraction ((18, 0) CNT)

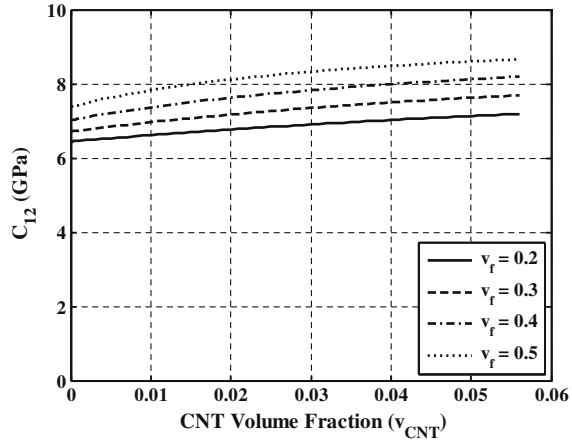

Fig. 24 Variation of the effective elastic coefficient C_{12} of the FFRC with the CNT volume fraction ((18, 0) CNT)

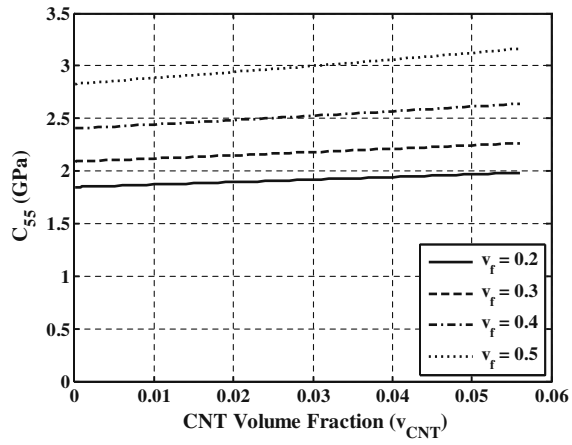

Fig. 25 Variation of the effective elastic coefficient C_{55} of the FFRC with the CNT volume fraction ((18, 0) CNT)

that the effective value of C_{22} is significantly sensitive to the change in CNT volume fraction. Although not shown here, similar trend of the results are also predicted for the effective elastic constant C_{23}. Figure 24 displays that the effective value of C_{12} increases marginally with the CNT volume fraction and the same is also true for the effective elastic constant C_{55} as shown in Fig. 25.

4 Conclusions

A novel fuzzy fiber reinforced composite (FFRC) is proposed which is composed of single-walled zig-zag CNTs, carbon fibers and polyimide matrix. The carbon fiber reinforcements are horizontally aligned and CNTs are radially grown on the surfaces of these carbon fibers. Two analytical models based on the micromechanics such as the mechanics of materials (MOM) approach and the Mori-Tanaka (MT) method are derived to predict the effective elastic properties of a lamina made of this proposed FFRC. The effective properties of the FFRC are estimated with and without the consideration of an interphase between a CNT and the polymer matrix. The interphase is a continuum representation of the non bonded van der Waals interaction between the atoms of CNTs and the atoms of the polymer matrix. In the absence of the interphase, it is assumed that CNT and the polymer matrix are perfectly bonded and the models are derived by the MOM approach and the two-phase MT method. The three-phase MT method

is employed to derive the model taking into account the effect of the interphase. Because of the constructional feature of the proposed FFRC, there exists a maximum value of the CNT volume fraction for a particular value of the carbon Þber volume fraction. Such maximum volume fraction of CNT increases with the increase in the diameter of the CNT. The present study reveals that the CNTs being radially grown on the surface of the carbon Þber with its axis normal to this surface, signiÞcantly improve the values of the transverse effective elastic constants C_{22}, C_{33}, C_{23}, C_{12}, C_{13} and C_{55} of the proposed FFRC over their values without CNTs. This is attributed to the fact that the elastic properties of CNT along its axis are exceptionally larger than those transverse to its axis and CNTs are transverse to the carbon Þber. The in-plane effective elastic coefÞcient C_{11} is not affected by the radial growing of CNTs on the surface of carbon Þbers. Although the consideration of the interphase between CNT and the polymer matrix was a concern, it does not affect the in-plane effective elastic coefÞcient C_{11} and its effects on the other effective elastic coefÞcients are also not pronounced. The predicted values of these effective elastic coefÞcients considering the interphase is slightly greater than those when perfectly bonding condition between the CNT and the polymer matrix is considered. Thus for conservative and intuitive estimates, one may neglect the non bonded van der Waals interaction between an atom of CNT and the polymer matrix and consider the perfect bond between a CNT and the polymer matrix. The effective values of the transverse elastic coefÞcients of the FFRC marginally increase with the increase in the CNT diameter as long as the carbon Þber volume fraction remains low. Since the transverse properties of the proposed FFRC are signiÞcantly improved without the cost of the values of the in-plane effective elastic constants C_{11}, the proposed FFRC will have better strength against the delamination failure. The present investigation will be useful for the experimental veriÞcation of the proposed FFRC.

Appendix

Equation30 as shown in the results and discussion section can be derived as follows:

Referring to Fig.6, the RVE of the FFRC can be considered as an equilateral triangle. Thus the volume (V^{FFRC}) of the RVE of the FFRC is given by

$$V^{FFRC} = \frac{\sqrt{3}}{4} D^2 L \qquad (31)$$

where $D = 2R$. The volume (V^f) of the carbon Þber is

$$V^f = \frac{\pi}{8} d^2 L \qquad (32)$$

where $d = 2a$. Thus the carbon Þber volume fraction (v_f) in the FFRC can be expressed as

$$v_f = \frac{V^f}{V^{FFRC}} = \frac{\pi}{2\sqrt{3}} \frac{d^2}{D^2} \qquad (33)$$

Using A (3), the carbon Þber volume fraction ($\bar{v}_f$) in the CFF can be derived as

$$\bar{v}_f = \frac{\frac{\pi}{8} d^2 L}{\frac{\pi}{8} D^2 L} = \frac{2\sqrt{3}}{\pi} v_f \qquad (34)$$

The maximum number (N_{CNT})$_{max}$ of radially grown aligned CNTs on the surface of the carbon Þber is given by

$$(N_{CNT})_{max} = \frac{\pi d L}{2(d_n + 1.7)^2} \qquad (35)$$

Therefore the volume (V^{CNT}) of the CNTs is

$$V^{CNT} = \frac{\pi}{4} d_n^2 (R - a)(N_{CNT})_{max} \qquad (36)$$

Thus the maximum volume fraction (v_{CNT})$_{max}$ of the CNT with respect to the volume of the FFRC can be determined as

$$(v_{CNT})_{max} = \frac{V^{CNT}}{V^{FFRC}} = \frac{\pi d_n^2}{2(d_n + 1.7)^2} \left(\sqrt{\frac{\pi v_f}{2\sqrt{3}}} - v_f \right) \qquad (37)$$

Finally, the maximum volume fraction (max (v_{nt})) of the CNTs with respect to the volume of the PMNC and with respect to the volume of the CFF (max ($\bar{v}_{nt}$)) can be determined in terms of max (v_{CNT}) as follows:

$$(v_{nt})_{max} = \frac{V^{CNT}}{V^{PMNC}} = \frac{2\sqrt{3}}{\pi} \frac{(D^2)}{(D^2 - d^2)} (v_{CNT})_{max} \qquad (38)$$

$$(\bar{v}_{nt})_{max} = \frac{V^{CNT}}{V^{CFF}} = \frac{2\sqrt{3}}{\pi} (v_{CNT})_{max} \qquad (39)$$

References

Batra, R.C., Sears, A.: Uniform radial expansion/contraction of carbon nanotubes and their transverse elastic moduli. Model. Simul. Mater. Sci. Eng. 15, 835–844 (2007)

Bevensite, Y., Dvorak, G.J.: Uniform fields and universal relations in piezoelectric composites. J. Mech. Phys. Solids 40, 1295–1312 (1992)

Cheng, H.C., Liu, Y.L., Hsu, Y.C., Chen, W.H.: Atomistic-continuum modeling for mechanical properties of single-walled carbon nanotubes. Int. J. Solids Struct. 46, 1695–1704 (2009)

Dunn, M.L., Ledbetter, H.: Elastic moduli of composites reinforced by multiphase particles. ASME J. Appl. Mech. 62, 1023–1028 (1995)

Esteva, M., Spanos, P.D.: Effective elastic properties of nanotube reinforced composites with slightly weakened interfaces. J. Mech. Mater. Struct. 4, 887–900 (2009)

Gao, X.L., Li, K.: A shear-lag model for carbon nanotube reinforced polymer composites. Int. J. Solids Struct. 42, 1649–1667 (2005)

Garcia, E.J., Wardle, B.L., Hart, A.J., Yamamoto, N.: Fabrication and multifunctional properties of a hybrid laminate with aligned carbon nanotubes grown in situ. Compos. Sci. Technol. 68, 2034–2041 (2008)

Gou, J., Minaie, B., Wang, B., Liang, Z., Zhang, C.: Computational and experimental study of interfacial bonding of single-walled nanotube reinforced composites. Comput. Mater. Sci. 31, 225–236 (2004)

Gupta, S.S., Batra, R.C.: Wall thickness and radial breathing modes of single-walled carbon nanotubes. ASME J. Appl. Mech. 75, 061010 (2008)

Honjo, K.: Thermal stresses and effective properties calculated for fiber composites using actual cylindrically-anisotropic properties of interfacial carbon coating. Carbon 45, 865–872 (2007)

Iijima, S.: Helical microtubules of graphitic carbon. Nature 354, 56–58 (1991)

Jiang, Y.L., Martin, L.D.: Anisotropic coupled-field inclusion and inhomogeneity problems. Philos. Mag. A 77(5), 1341–1350 (1998)

Jiang, B., Liu, C., Zhang, C., Liang, R., Wang, B.: Maximum nanotube volume fraction and its effect on overall elastic properties of nanotube-reinforced composites. Composites B 40, 212–217 (2009)

Li, C., Chou, T.W.: A structural mechanics approach for the analysis of carbon nanotubes. Int. J. Solids Struct. 40, 2487–2499 (2003)

Lu, J.P.: Elastic properties of carbon nanotubes and nanoropes. Phys. Rev. Lett. 79, 1297–1300 (1997)

Mathur, R.B., Chatterjee, S., Singh, B.P.: Growth of carbon nanotubes on carbon fiber substrates to produce hybrid/phenolic composites with improved mechanical properties. Compos. Sci. Technol. 68, 1608–1615 (2008)

Meguid, S.A., Zhu, Z.H.: A novel finite element for treating inhomogeneous solids. Int. J. Numer. Methods Eng. 38, 1579–1592 (1995)

Meguid, S.A., Wernik, J.M., Cheng, Z.Q.: Atomistic-based continuum representation of the effective properties of nano-reinforced epoxies. Int. J. Solids Struct. 47, 1723–1736 (2010)

Mori, T., Tanaka, K.: Average stress in matrix and average elastic energy of materials with misfitting inclusions. Acta Metall. 21, 571–574 (1973)

Odegard, G.M., Gates, T.S., Wise, K.E., Park, C., Siochi, E.J.: Constitutive modeling of nanotube-reinforced polymer composites. Compos. Sci. Technol. 63, 1671–1687 (2003)

Odegard, G.M., Clancy, T.C., Gates, T.S.: Modeling of the mechanical properties of nanoparticle/polymer composites. Polymer 46, 553–562 (2005)

Qui, Y.P., Weng, G.J.: On the application of Mori-Tanaka's theory involving transversely isotropic spheroidal inclusions. Int. J. Eng. Sci. 28(11), 1121–1137 (1990)

Ray, M.C.: Concept for a novel hybrid smart composite reinforced with radially aligned zigzag carbon nanotubes on piezoelectric fibers. Smart Mater. Struct. 19, 035008 (2010)

Ray, M.C., Batra, R.C.: Effective properties of carbon nanotube and piezoelectric fiber reinforced hybrid smart composite. ASME J. Appl. Mech. 76, 034–503 (2009)

Ray, M.C., Guzman de Villoria, R., Wardle, B.L.: Load transfer analysis in short carbon fibers with radially-aligned carbon nanotubes embedded in a polymer matrix. J. Adv. Mater. 41(4), 82–94 (2009)

Rio, T.G., Poza, P., Rodriguez, J., Garcia, M.C., Hernandez, J.J., Ezquerra, T.A.: Influence of single-walled carbon nanotubes on the effective elastic constants of poly (ethylene terephthalate). Compos. Sci. Technol. 70, 284–290 (2010)

Shen, L., Li, J.: Transversely isotropic elastic properties of single-walled carbon nanotubes. Phys. Rev. B 69, 045–414 (2004)

Smith, W.A., Auld, B.A.: Modeling 1–3 composite piezoelectrics: thickness mode oscillations. IEEE Trans. Ultrason. Ferroelectr. Freq. Control 38(1), 40–47 (1991)

Song, Y.S., Youn, J.R.: Modeling of effective elastic properties for polymer based carbon nanotube composites. Polymer 47, 1741–1748 (2006)

Thostenson, E.T., Chow, T.W.: On the elastic properties of carbon nanotube based composites: modeling and characterization. J. Phys. D 36, 573–582 (2003)

Treacy, M.M.J., Ebbessen, T.W., Gibson, J.M.: Exceptionally high Young's modulus observed for individual carbon nanotubes. Nature 381, 678–680 (1996)

Tsai, J.L., Tzeng, S.H., Chiu, Y.T.: Characterizing elastic properties of carbon nanotube/polyimide nanocomposites using multi-scale simulation. Composites B 41, 106–115 (2010)

Wernik, J.M., Meguid, S.A.: Multiscale modeling of the nonlinear response of nano-reinforced polymers. Acta Mech. 217, 1–16 (2011)

Xiao, J.R., Gama, B.A., Gillespie, J.W.: An analytical molecular structural mechanics model for the mechanical properties of carbon nanotubes. Int. J. Solids Struct. 42, 3075–3092 (2005)

Zhang, J., He, C.: A three-phase cylindrical shear-lag model for carbon nanotube composites. Acta Mech. 196, 33–54 (2008)

Zhang, Q., Qian, W., Xiang, R., Yang, Z., Luo, G., Wang, Y., Wei, F.: In situ growth of carbon nanotubes on inorganic fibers with different surface properties. Mater. Chem. Phys. 107, 317–321 (2008)